Pressure-Induced Structural Phase Transition of Co-Doped SnO2 Nanocrystals

Vinod Panchal *, Laura Pampillo, Sergio Ferrari, Vitaliy Bilovol, Catalin Popescu, Daniel Errandonea *

Posted Date: 15 May 2023

doi: 10.20944/preprints202305.1025.v1

Keywords: High Pressure; Phase Transition; Synchrotron Radiation, X-ray Diffraction

Article

Pressure-Induced Structural Phase Transition of Co-Doped SnO_2 Nanocrystals

V. Panchal [1], L. Pampillo [2], S. Ferrari [2], V. Bilovol [2,3], C. Popescu [4] and D. Errandonea [5,*]

[1] Department of Physics, Royal College, Mumbai-401107, India; panchalvinod@yahoo.com
[2] Universidad de Buenos Aires, Consejo Nacional de lnvestigaciones Científicas y Técnicas. Instituto de Tecno-logía y Ciencias de la Ingeniería Ing. Hilario Fernández Long (INTECIN). Av. Paseo Colón 850, C1063ACV, Ciudad Autónoma de Buenos Aires, Argentina
[3] Academic Centre for Materials and Nanotechnology, AGH University of Science and Technology, Al. Mickie-wicza 30, 30-059 Krakow, Poland
[4] ALBA-CELLS, Cerdanyola del Vallès, Barcelona, Spain
[5] Departamento de Física Aplicada, Instituto de Ciencias de Materiales, MALTA Consolider team, Universitat de Valencia, 46100 Valencia, Spain
* Correspondence: daniel.errandonea@uv.es

Abstract: Co-doped SnO2 nanocrystals with tetragonal rutile-type (space group P42/mnm) structure have been investigated using in-situ high-pressure synchrotron angle dispersive X-ray diffraction till 20.9 GPa at ambient temperature. The analysis of experimental results based on Rietveld refinements suggest that rutile-type SnO2 undergoes a structural phase transition at 14.2 GPa to an orthorhombic CaCl2-type phase (space group Pnnm) with no coexistence during the phase transition. No further phase transition is observed till 20.9 GPa. The low-pressure and high-pressure phases are related via a group/subgroup relationship. However, as a discontinuous change in the unit-cell volume is detected at the phase transition, thus, the phase transition can be classified as first-order type. On decompression the transition is found to be re-versible. The results are compared with previous high-pressure studies on SnO2.

Keywords: high pressure; phase transition; synchrotron radiation; X-ray diffraction

1. Introduction

Nano-scale materials are having a great impact in human life. They are changing dental medicine, healthcare, and human life more profoundly than several developments of the past. Nanomaterials research has also become a striking area of research due to their intriguing chemical and physical properties. Nanomaterials are preferred over their bulk counterpart due to enhancement in catalytic, optical, magnetic, and electrical properties [1-3]. The nature of pressure-induced structural phase transitions, elastic properties, and transition pressure in nanomaterials are quite different compared to the bulk materials [4-9]. Tin dioxide (SnO_2) is a technologically very important material and a widely used wide bandgap semiconductor. It finds applications in the field of solar cells [10], ultraviolet photodetectors [11], short wavelength light-emitting diodes [12], spintronic applications [13], gas sensors [14], and lithium-ion batteries [15].

At ambient conditions SnO_2, which is also known as stannic oxide, crystallizes in a crystal structure isomorphic to tetragonal rutile (space group $P4_2/mnm$, $Z = 2$). In this structure two Sn ions are six-fold coordinated by oxygen atoms, which are shared with adjacent SnO_6 octahedra as shown in Figure 1(a). In the past, it has been reported that SnO_2 undergoes the following sequence of pressure-induced structural phase transitions: rutile-type phase → $CaCl_2$-type phase → PbO_2-type phase → fluorite-type phase [16]. Earlier high-pressure (HP) X-ray diffraction (XRD) measurements [16-17], theoretical *ab-initio* calculations [18-22], and HP Raman scattering [23] on bulk as well as nanocrystalline samples indicate the occurrence of a second order-structural phase transition between 7-14 GPa, from the tetragonal rutile-type to the orthorhombic $CaCl_2$-type structure (space group *Pnnm*), which is represent in Figure 1(b)). In the $CaCl_2$-type structure, the Sn atoms are also octahedrally coordinated by oxygen atoms, forming chains of edge-sharing octahedra along the *c*-axis of the structure, while perpendicular to the *c*-axis two octahedra are linked by sharing one corner.

Preprints (www.preprints.org) | NOT PEER-REVIEWED | Posted: 15 May 2023 doi:10.20944/preprints202305.1025.v1

However, there are few exceptions for the rutile to $CaCl_2$-type transition. For example, high-pressure XRD measurement carried out on nanocrystalline 5-nm sized samples [24] and 8-nm sized samples [25-26] indicated a direct tetragonal rutile to cubic fluorite first-order structural phase transition beyond 18 GPa. The transition pressure was also found to be increased with decreasing particle size [26]. Even doping has shown alteration in the high-pressure behavior, elastic properties, and optical properties. For example, in Fe-doped nanoparticles (size 18 nm and 10 at % doping) of SnO_2 shows an increase in the transition pressure and bulk modulus [27] whereas V-doped nanoparticles (size 10 - 30 nm and 5 - 12.5 at % doping) of SnO_2 shows a decrease in the bulk modulus with increasing concentration of the dopant [28]. Hence, it is very interesting to know how the particle size, doping concentration, and type of doping ion are altering the high-pressure behavior and elastic properties of SnO_2, and further systematic investigations are required in this direction. In the current contribution, we are reporting HP synchrotron XRD studies up to 20.9 GPa on Co-doped nanocrystalline SnO_2 (crystallite size 15 nm and 10 at % doping) to contribute to the understanding of the effect of doping on the transition pressure and elastic properties. Such kind of study is not reported earlier.

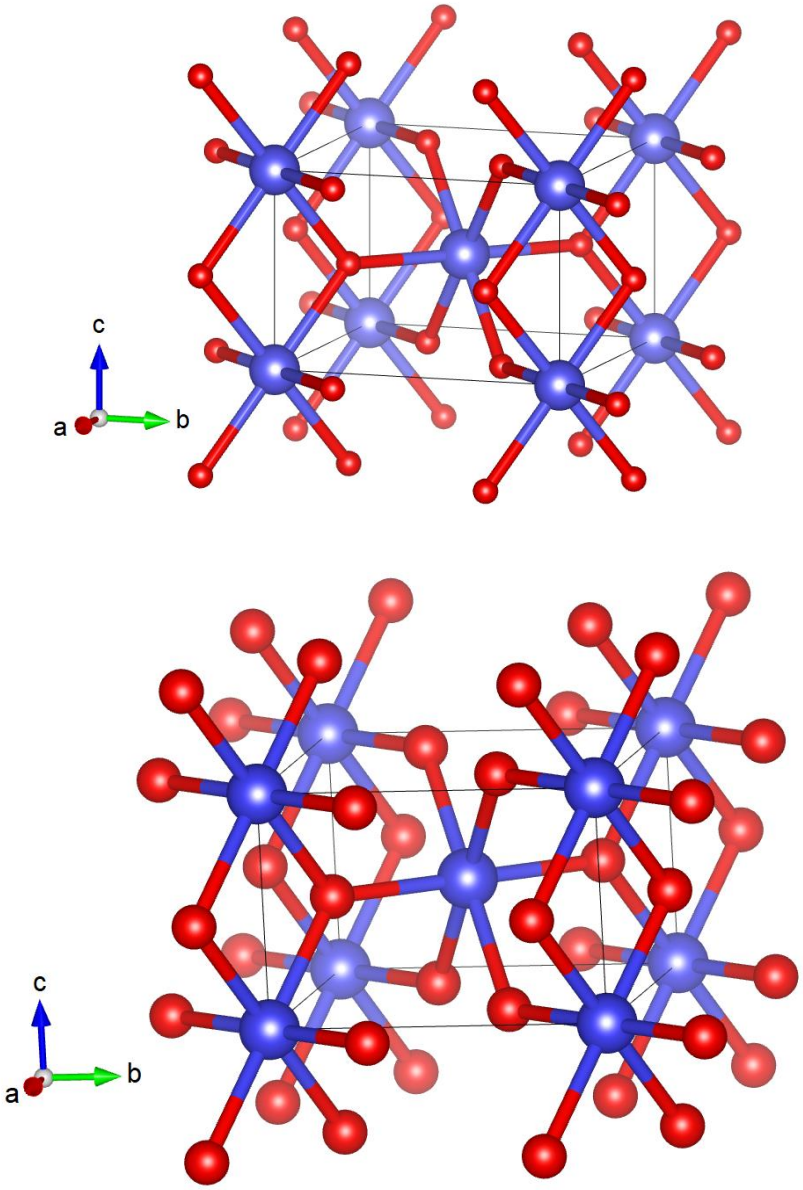

Figure 1. Schematic view of (a) tetragonal rutile-type SnO_2, space group $P4_2/mnm$ and (b) orthorhombic SnO_2, space group $Pnnm$ (Sn^{+4} cations are in blue and O^{-2} anions in red).

Preprints (www.preprints.org) | NOT PEER-REVIEWED | Posted: 15 May 2023 doi:10.20944/preprints202305.1025.v1

2. Experiments

Cobalt-doped SnO_2 nanoparticles were prepared by the wet chemical co-precipitation method following the procedure described by Ferrari *et al.* [29]. To implement the cobalt doping we used cobalt chloride from Sigma-Aldrich. The nanoparticles were characterized at ambient-conditions by means of powder XRD confirming the formation of single-phase rutile-type nanoparticles with unit-cell parameters a = 4.732(1) Å and c = 3.185(1) Å, which are consistent with single crystal X-ray diffraction studies on bulk SnO_2 [30-31]. The average particle size of 15 nm was determined from XRD using the Scherrer equation [32]. The cobalt concentration (10 at %) was determined from Energy-dispersive X-ray spectroscopy. HP powder XRD measurements were carried out at the MSPD-BL04 beamline of ALBA synchrotron using a monochromatic beam of wavelength 0.4642 Å. The beam was focused down to a 20 μm full-width-at-half-maximum spot. A Rayonix charge-coupled device detector was used to collect XRD patterns. The detector was calibrated using LaB_6 as standard. Two-dimensional diffraction rings obtained from the detector were transformed into one-dimensional diffractograms using Dioptas. Measurements were performed with a membrane diamond-anvil cell (DAC) equipped with 500-μm diameter diamond anvils. We used a stainless-steel gasket pre-indented to a thickness of 40 μm with a centered hole of 200 μm in diameter. As pressure-transmitting medium we used a 16:3:1 methanol–ethanol–water mixture, which remains quasi-hydrostatic up to 10 GPa [33]. The pressure was determined using the equation of state (EOS) of copper (Cu) [34] with a precision of ±0.05 GPa. The structural analysis was performed by employing the Rietveld technique using Fullprof [35].

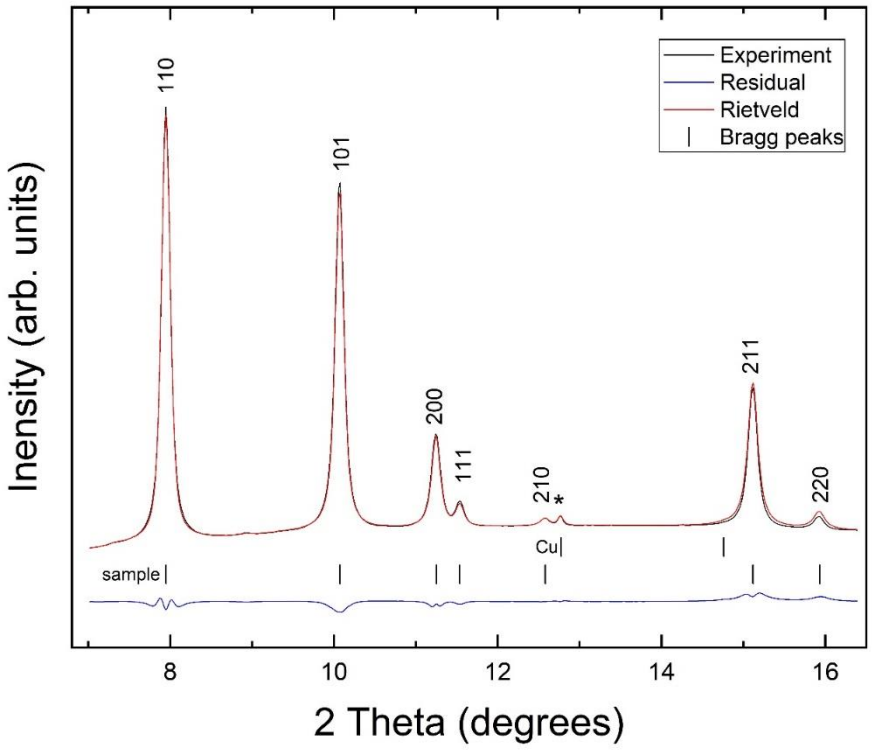

Figure 2. The Rietveld profile fit for tetragonal rutile-type phase at 0.6 GPa. The asterisk (*) is the (111) diffraction peak of copper used to determine pressure. The vertical bars indicate the calculated positions of diffraction peaks of the sample.

3. Results and Discussion

Figure 2 shows the powder XRD pattern at the lowest pressure measured in the DAC (0.6 GPa) including the Rietveld refinement. The diffraction pattern can be undoubtedly assigned to the rutile-type structure. In the pattern there is an extra weak peak denoted by the asterisk symbol (*) which is assigned to the copper grain used as pressure marker. The unit-cell parameters at 0.6 GPa are a =

Preprints (www.preprints.org) | NOT PEER-REVIEWED | Posted: 15 May 2023 doi:10.20944/preprints202305.1025.v1

4.728(1) Å and c = 3.184(1) Å. The goodness of fit parameters are Rwp = 6.16 %, Rp = 3.4 %. Figure 3 shows XRD patterns of nanocrystalline Co-doped SnO_2 at representative pressures.

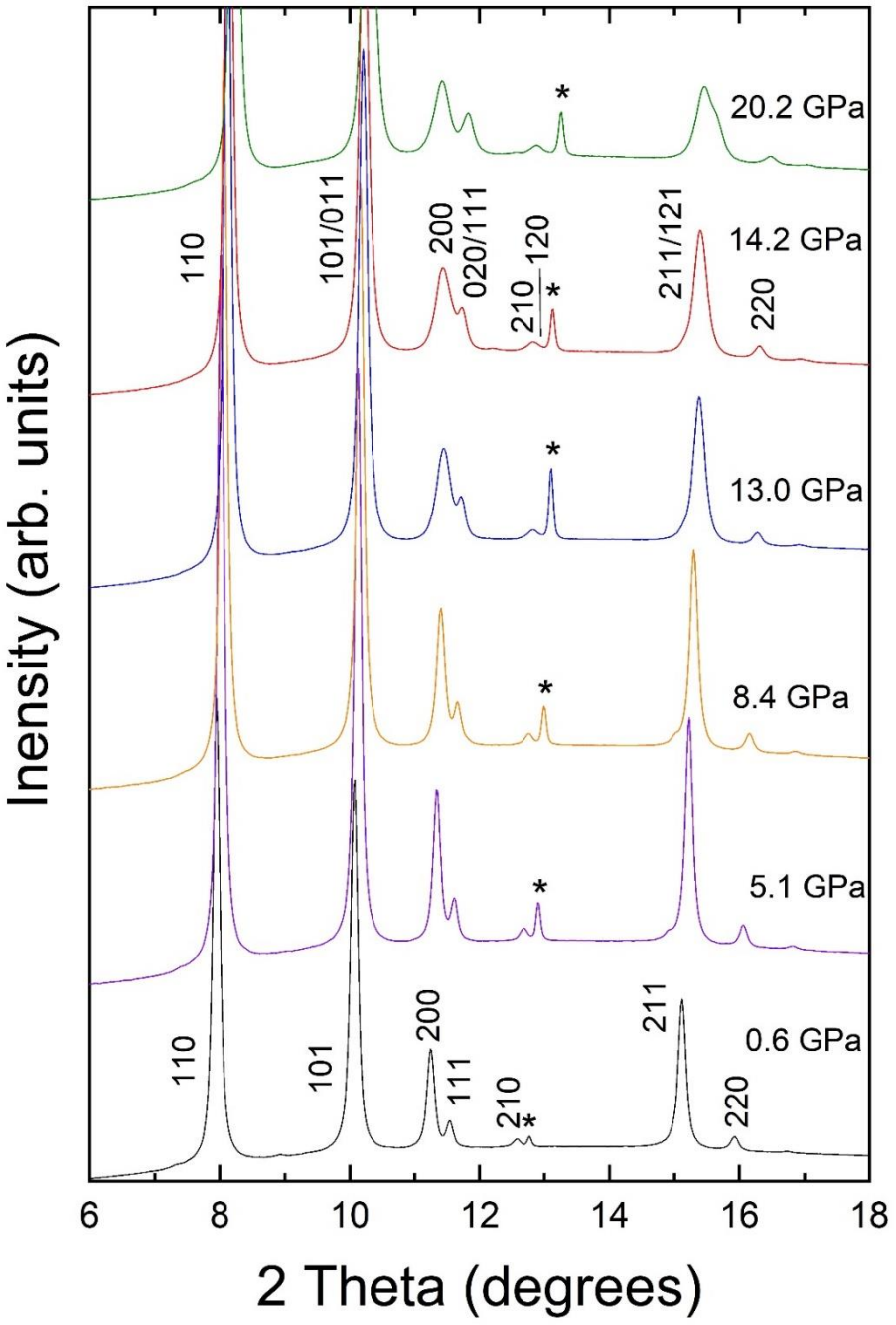

Figure 3. X-ray powder diffraction patterns of SnO2 at representative pressures. The asterisk (*) is the (111) diffraction peaks of copper. The initial and first high-pressure phase have been indexed with the tetragonal rutile and the orthorhombic CaCl2-type structure respectively.

There are no noticeable changes in the diffraction patterns up to 13 GPa, other than peaks shift to higher angle due to the contraction of unit-cell parameters. All the diffraction peaks up to 13 GPa could be successfully indexed to the low-pressure (LP) rutile-type phase. In addition to the peaks assigned to SnO_2, a peak due to copper (marked by *), used to determine pressure, can be identified in all the x-ray diffraction profiles. We have observed a systematic shift in all the diffraction peaks to higher 2θ due to lattice compression. At 14.2 GPa we have observed few discernible changes in the diffraction profile, which are indicative of a phase transformation. The cell metric is no longer

Preprints (www.preprints.org) | NOT PEER-REVIEWED | Posted: 15 May 2023 doi:10.20944/preprints202305.1025.v1

consistent with $P4_2/mnm$ symmetry and another crystallographic phase with symmetry $Pnmm$ occurs, corresponding to orthorhombic $CaCl_2$-type structure. In particular, at the pressure of 14.2 GPa, the broadening of the (101) and (111) diffraction peaks of rutile along with the splitting of the (210) diffraction peak were observed. The diffraction profile could not be well indexed to tetragonal rutile-type phase. On the other hand, the orthorhombic $CaCl_2$-type structure gives the correct positions of diffraction peaks as indicated by unbiased refinements. Furthermore, this structural phase transition agrees with earlier investigations on rutile SnO_2 [16-22].

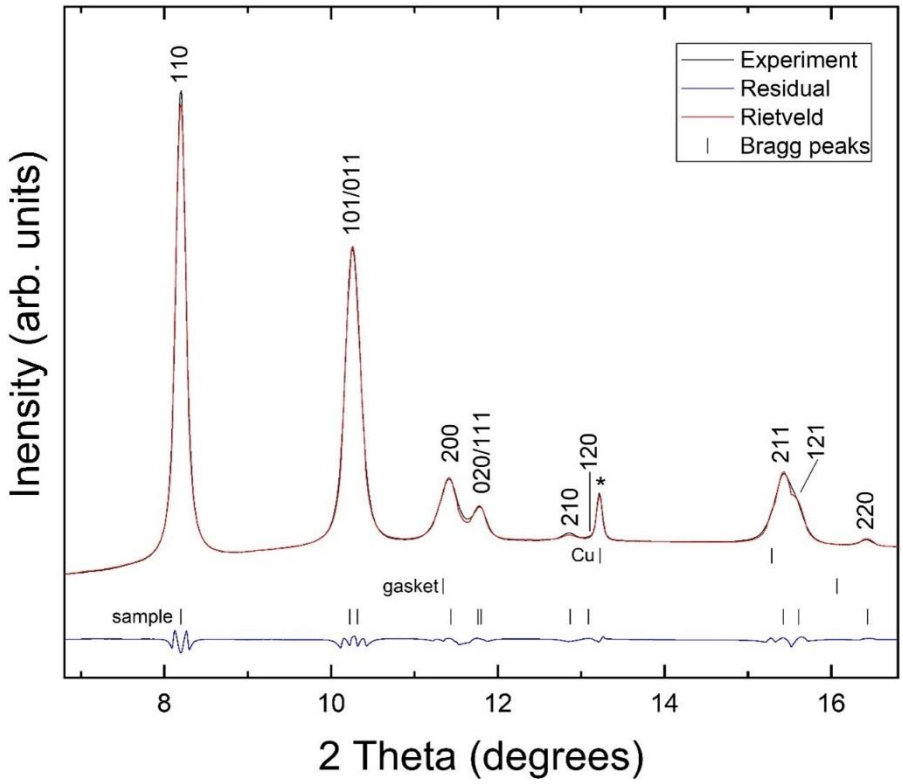

Figure 4. The Rietveld profile fit at 14.2 GPa for the orthorhombic $CaCl_2$-type phase. The asterisk (*) is the (111) diffraction peak of copper used to determine pressure. The vertical bars indicate the calculated positions of diffraction peaks of sample. The contributions from the gasket and copper also indicated.

On further increase of pressure, the orthorhombic $CaCl_2$-type structure continues stable till 20.9 GPa, which is the highest pressure in this investigation. On release of pressure, we have found that the phase transition is reversible. In the experiment, we have not observed any coexistence of phases. This and the group-subgroup relationship between space groups $P4_2/mnm$ and $Pnnm$ suggest that the transition could be of second-order in nature, which agrees with conclusions from previous XRD measurements on doped and un-doped nanocrystalline SnO_2 [27]. However, as we will explain below, at the phase transition, we have detected a volume discontinuity, which undoubtedly supports a first-order nature for the phase transition in Co-doped SnO_2. Notice that up to now this is the only SnO_2 nanomaterial where such a volume discontinuity has been detected. We speculate it could be related to changes in the strong anti-ferromagnetic super-exchange interaction between Co ions that exist in Co-doped SnO_2 [36]. Another hypothesis to explain the abrupt volume collapse is the influence of structural defects that are induced by Co-doping [37]. Additional studies are needed to fully understand the distinctive behavior of Co-dopen SnO_2. The Rietveld refinement of the XRD patterns profile measured for the HP phase at 14.2 GPa is shown in Fig. 4. In addition to the peaks from the sample and Cu, we observed a weak contribution of the gasket, which makes the peak (200) of the HP phase to become asymmetric. The unit-cell parameters of the HP phase at 14.2 GPa are a = 4.675(2) Å, b = 4.572(3) Å, and c = 3.151(1) Å. The goodness of fit parameters are Rwp = 9.84 % and Rp = 7.79 %.

Preprints (www.preprints.org) | NOT PEER-REVIEWED | Posted: 15 May 2023 doi:10.20944/preprints202305.1025.v1

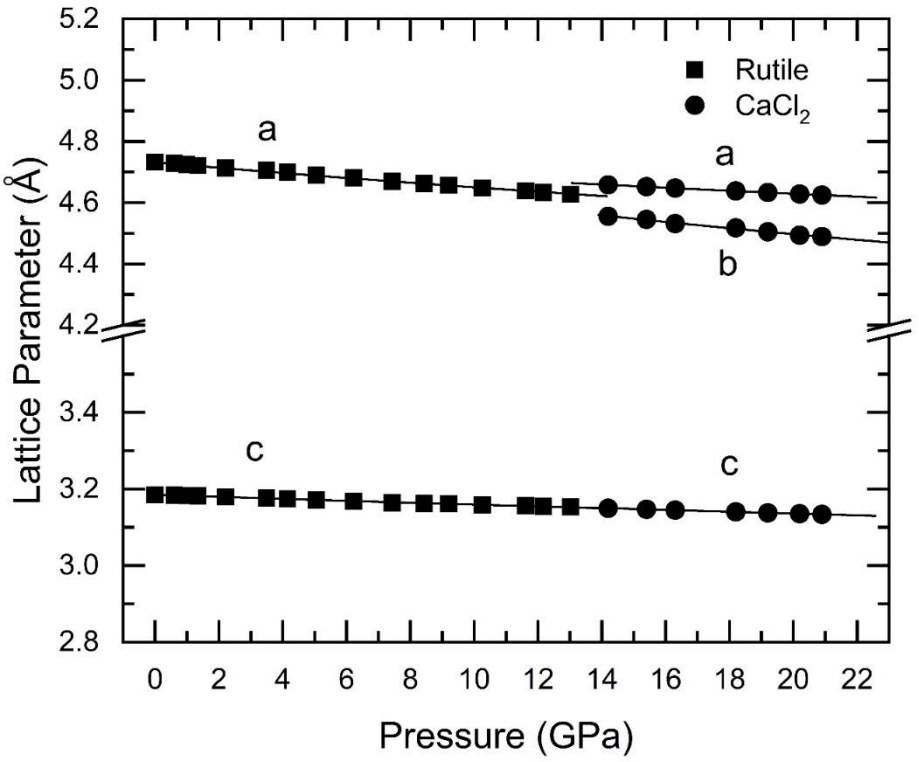

Figure 5. Pressure dependance of lattice parameters of Co-doped SnO_2. Solid squares represent the tetragonal rutile-type phase and solid circles represent the orthorhombic $CaCl_2$-type structure. Solid lines are linear fits of lattice parameters.

The pressure evolution of the lattice parameters of Co-doped nanocrystalline SnO_2 in the tetragonal rutile-type and orthorhombic $CaCl_2$-type phases is shown in Fig. 5. The pressure dependence of the unit-cell volume is reported in Fig. 6. We have observed a discontinuity in volume ($-\Delta V/V \sim 1.0\%$) at the transition pressure, indicating a first-order nature of the structural phase transition. Using the EOSFIT software [38] the linear compressibility of each phase was calculated. We have observed that in the rutile-type phase SnO_2 the axial compressibilities are highly anisotropic. The *a*-axis is more compressible than the *c*-axis, as is evident from the increase of the *c*/*a* ratio from 0.673 at ambient pressure to 0.681 at 13 GPa. The linear compressibility of the *c*-axis is found to be $K_c = 1.02(4) \times 10^{-3}$ GPa^{-1}, which is almost half than a-axes compressibility $K_a = 1.72(6) \times 10^{-3}$ GPa^{-1}. This anisotropic behavior in compressibility is in quite agreement with earlier reported values of bulk SnO_2 samples [30, 39, 40] and even for un-doped, Fe-doped, and V-doped nanocrystalline SnO_2 [27-28]. However, the values of axial compressibility obtained in this investigation are slightly higher compared to earlier investigations [27, 28, 30, 39, 40]. In case of orthorhombic $CaCl_2$-type phase the axial compressibilities are found to be highly anisotropic as well, the b-axis is more compressible compared to other two axes. The linear compressibility of all the three axes is found to be as $K_a = 1.65(4) \times 10^{-3}$ GPa^{-1}, $K_b = 1.90(1) \times 10^{-3}$ GPa^{-1} and $K_c = 1.05(2) \times 10^{-3}$ GPa^{-1}.

Preprints (www.preprints.org) | NOT PEER-REVIEWED | Posted: 15 May 2023 doi:10.20944/preprints202305.1025.v1

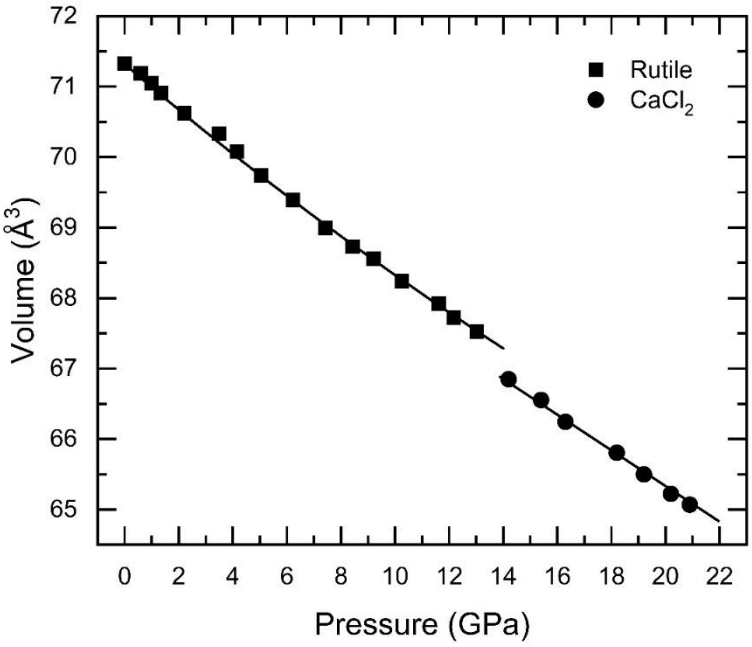

Figure 6. Volume versus Pressure data for Co-doped SnO_2. Solid squares represent the tetragonal rutile-type phase and solid circles represent the orthorhombic $CaCl_2$-type structure. Solid lines represent Birch-Murnaghan fit to the data for both phases.

The *P*–*V* data of the rutile phase of SnO_2 in the tetragonal phase, fitted to the second-order Birch–Murnaghan equation of state, gives the bulk modulus to be B_o = 213(9) GPa with B_0' = 4. During this fit the bulk modulus B_o and ambient pressure volume V_o are kept as free variables. This value is in a good agreement with previously reported values for bulk [16], and even for un-doped, Fe-doped nanocrystalline SnO_2 [27]. These values are summarized in Table 1. However, in V-doped nanocrystalline samples bulk modulus is found to be decreasing with increasing doping concentrations, in the range of 185-142 GPa [28]. We can conclude that in contrast with V-doping, a 10% doping with Co and Fe does not affect the mechanical properties of SnO_2. A possible reason for it, it could be the fact that V has larger ionic radii than Fe and Co. For the high-pressure phase the bulk modulus obtained is B_0 = 228(9) GPa. The slight increase of the bulk modulus at the phase transition is consistent with the fact that the HP phase is denser than the low-pressure phase due to the volume contraction observed at the transition. However, both bulk moduli agree within error bars; 213(9) and 228(9) GPa. In this regard, the behavior is more similar to the behavior of bulk SnO_2 [16], where no changes are detected in the bulk modulus at the transition (see Table 1), than to the behavior of the bulk modulus for Fe-doped and V-doped nanocrystalline SnO_2 [27-28], where a 15 % increase of the bulk modulus was reported after the transition. At the moment, it is not clear that the different behavior is inherent to the different doping or to difference on non-hydrostatic stresses in experiments [41]. Future studies are needed to clarify this issue. On the other hand, it should be noticed that in the equation of state, the volume at zero pressure (V_0) and B_0 are correlated. Then, large uncertainties on V_0 could affect the value of B_0 [42]. This can be the case of SnO_2, where the phase transition is reversible and therefore no data is available for the HP phase at pressures close to ambient pressure. This means that the determination of V_0 comes from the extrapolation of data measured above 14 GPa, which could lead to large errors in the determination of V_0 which will necessarily propagate to the determination of B_0.

Table 1. Bulk modulus determined for different phase of nanocrystalline of SnO_2. We include results from this work and for the literature [16, 17, 24, 26, 27, 28].

Sample	Bulk Modulus (GPa) Rutile-type SnO_2	Bulk Modulus (GPa) $CaCl_2$-type SnO_2	Ref.

Bulk	205	204	17
Bulk	252	----	26
Bulk	205	204	16
Nanocrystalline (5nm)	217	---	24
Nanocrystalline (3nm)	233	---	26
Nanocrystalline (30nm)	210	252	27
Nanocrystalline Fe-doped (18nm)	213	256	27
Nanocrystalline V-doped (13nm)	185	--	28
Nanocrystalline Co-doped (15nm)	213(9)	228(9)	This work

4. Conclusions

In summary, our in-situ synchrotron powder x-ray diffraction study on nanocrystalline Co-doped SnO_2 shows that it undergoes a first-order structural phase transition from the tetragonal rutile to the orthorhombic $CaCl_2$-type phase at ~14.2 GPa. The crystal structure of the high-pressure phase is the same high-pressure structure observed in bulk, doped and undoped nanocrystalline samples of SnO_2. We have not observed any coexistence of phases during the phase transition. The compressibility behavior was found to be highly anisotropic in both phases, and the value of bulk modulus for the tetragonal rutile phase is in good agreement with earlier measurements. However, for orthorhombic $CaCl_2$-type phase there our bulk modulus is 10 % smaller than the same parameter in Fe- and V-doped SnO_2. The high-pressure phase was observed to remain stable till 20.9 GPa. On release of pressure the phase transition is found to be reversible.

Author Contributions: Conceptualization, D.E.; methodology, validation, V.P. and D.E. Formal analysis, V.P., S.F., D.E.; investigation, V.P., L.P., S.F., V.B., C.P., and D.E.; writing—original draft preparation, V.P..; writing—review and editing, V.P., L.P., S.F., V.B., C.P., and D.E.; supervision, D.E. All authors have read and agreed to the published version of the manuscript.

Funding: D.E. thanks the financial support from Generalitat Valenciana under Grant PROMETEO CIPROM/2021/075-GREENMAT, the Advanced Materials Programme supported by MCIN and GVA with funding from European Union NextGenerationEU (PRTR-C17.I1) under grant MFA/2022/007, and by the Spanish Research Agency (AEI) and Spanish Ministry of Science and Investigation (MCIN) under projects PID2019-106383GB-C41 (DOI: 10.13039/501100011033) and RED2018-102612-T (MALTA Consolider-Team Network).

Data Availability Statement: Data are available upon reasonable request to corresponding author at daniel.errandonea@uv.es (D.E.).

Acknowledgements: The authors are grateful for financial support from the Spanish Research Agency (AEI) and Spanish Ministry of Science and Investigation (MCIN) under Grants PID2019-106383GB-41/43 (http://dx.doi.org/10.13039/501100011033) and RED2018-102612-T (MALTA Consolider Team Network) and from Generalitat Valenciana under Grant PROMETEO CIPROM/2021/075-GREENMAT. This study forms part of the Advanced Materials program and was supported by MCIN with funding from European Union Next Generation EU (PRTR-C17.I1) and by Generalitat Valenciana, Grant MFA/2022/007. The authors thank ALBA synchrotron for providing beam time for the XRD experiments (Proposal 2021085226).

Conflicts of Interest: The authors declare no conflict of interest.

References

1. Gleiter, H.; Nanocrystalline materials. *Prog. Mat. Science* **1989,** *33*, 223-315.
2. Siegel, R.; Cluster-assembled nanophase materials. *Annual Review of Materials Science* **1991**, *21*, 559-578.
3. Kodama, R.; Magnetic Nanoparticles. *J. Magn. Magn. Mat.* **1999**, *200*, 359-372.

4. Lv, H.; et al., Effect on grain size on pressure-induced structural transition in Mn_3O_4. *J. Phys. Chem. C* **2012**, *116*, 2165-2171
5. Srihari, V.; Verma, A.; Pandey, K.; Vishwanadh, B.; Panchal, V.; Garg, N.; Errandonea, D.; Making $Yb_2Hf_2O_7$ Defect Fluorite Uncompressible by Particle Size Reduction. *J. Phys. Chem. C* **2021**, *125*, 27354-27362.
6. Jiang, J.; Gerward, L.; Frost, D.; Secco, R.; Peyronneau, J.; Olsen, J.; Grain-size effect on pressure-induced semiconductor-to-metal transition in ZnS. *J. Appl. Phys.* **1999**, *86*, 6608-6610.
7. Wang, Z.; Tait, K.; Zhao, Y.; Schiferl, D.; Zha, C.; Uchida, H.; Downs, R.; Size- induced reduction of transition pressure and enhancement of bulk modulus of AlN Nanocrystals. *J. Phys. Chem. B* **2004**, *108*, 11506-11508.
8. Wang, Z.; Saxena, S.; Pischedda, V.; Liermann, H.; Zha, C.; In situ x-ray diffraction study of the pressure-induced phase transformation in nanocrystalline CeO_2. *Phys. Rev. B* **2001**, *64*, 012102.
9. Zvoriste-Walters, C.; Heathman, S.; Jovani-Abril, R.; Spino, J.; Janssen, A.; Caciuffo, R.; Crystal size effect on the compressibility of nano-crystalline uranium dioxide. *J. Nucl. Mater.* **2013**, *435*, 123-127.
10. Bouras, K.; Schmerber, G.; Rinnert, H.; Aureau, D.; Park, H.; Ferblantier, G.; Colis, S.; Fix, T.; Park, C.; Kim, W.; Dinia, A.; Slaoui, A.; Structural, optical and electrical properties of Nd-doped SnO_2 thin films fabricated by reactive magnetron sputtering for solar cell devices. *Sol. Energy Mater. Sol. Cells* **2016**, *145*, 134-141.
11. Wu, J.; Kuo, C.; Ultraviolet photodetectors made from SnO_2 nanowires. *Thin Solid Films* **2009**, *517*, 3870-3873
12. Tsai, M.; Bierwagen, O.; Speck, J.; Epitaxial Sb-doped SnO_2 and Sn-doped In_2O_3 transparent conducting oxide contacts on GaN-based light emitting diodes. *Thin Solid Films* **2016**, *605*, 186-192.
13. Ogale, S.; Choudhary, R.; Buban, J.; Lofland; S.; Shinde, S.; Kale, S.; Kulkarni, V.; Higgins, J.; Lanci, C.; Simpson, J.; Browning, N.; Sarma, S.; Drew, H.; Greene, R.; Venkatesan, T.; High Temperature Ferromagnetism with a Giant Magnetic Moment in Transparent Co-doped $SnO_{2-\delta}$. *Phys. Rev. Lett.* **2003**, *91*, 077205
14. Tadeev, A.; Delabouglise, G.; Labeau, M.; Influence of Pd and Pt additives on the microstructural and electrical properties of SnO_2-based sensors. *Mater. Sci. Eng. B* **1998**, *57*, 76-83.
15. Chandra, A.; Kalpana, D.; Thangadurai, P.; Ramasamy, S.; Synthesis and characterization of nanocrystalline SnO_2 and fabrication of lithium cell using nano-SnO_2. *J. Power Sources* **2002**, *107*, 138-141.
16. Haines, J.; Leger, J.; X-ray diffraction study of the phase transitions and structural evolution of tin dioxide at high pressure: Relationships between structure types and implications for other rutile-type dioxides. *Phys. Rev. B* **1997**, *55*, 11144
17. Shieh, S.; Kubo, A.; Duffy, T.; Prakapenka, V.; Guoyin, G.; High pressure phases in SnO_2 to 117 GPa. *Phys. Rev. B* **2006**, *73*, 14105.
18. Parlinski, K.; Kawazoe, Y.; Ab Initio study of phonons in the rutile structure of SnO_2 under pressure. *Eur. Phys. J. B* **2000**, *13*, 679-683.
19. Hassan, F.; Alaeddine, A.; Zoaeter, M.; Rachidi, I.; First-principles investigation of SnO_2 at high pressure. *Inter. J. of Mod. Phys. B* **2005**, *19*, 4081-4092.
20. Gracia, L.; Beltran, A.; Andres, J.; Characterization of high-pressure structures and phase transformations in SnO_2. A density functional theory study. *J. Phys. Chem. B* **2007**, *111*, 6479-6485.
21. Casali, R.; Lasave, J.; Caravaca, M.; Koval, S.; Ponce, C.; Migoni, R.; Ab initio and shell model studies of structural, thermoelastic and vibrational properties of SnO_2 under pressure. *J. Phys.: Condens. Matter* **2013**, *25*, 135404
22. Yang, L.; Weiliu, F.; Yanlu, L.; Wei, L.; Zhao, X.; Pressure induced ferroelastic phase transition in SnO_2 from density functional theory. *J. Chem. Phys.* **2014**, *140*, 164706.
23. Hellwig, H.; Goncharov, A.; Gregoryanz, E.; Mao, H.; Hemley, R.; Brillouin and Raman spectroscopy of the ferroelastic rutile-to-$CaCl_2$ transition in SnO_2 at high pressure. *Phys. Rev. B* **2003**, *67*, 174110.
24. Garg, A.; Pressure induced volume anomaly and structural phase transition in nanocrystalline SnO_2. *Phys. Status Solidi B* **2014**, *251*, 1380-1385.
25. Jiang, J.; Gerward, L.; Olsen, J.; Pressure induced phase transformation in nanocrystal SnO_2. *Scr. Mater.* **2001**, *44*, 1983-1986.
26. He, Y.; Liu, J.; Chen, W.; Wang, Y.; Wang, H.; Zeng, Y.; Zhang, G.; Wang, L.; Liu, J.; Hu, T.; Hahn, H.; Gleiter, H.; Jiang, J.; High pressure behavior of SnO_2 nanocrystals. *Phys. Rev. B* **2005**, *72*, 212102.
27. Grinblat, F.; Ferrari, S.; Pampillo, L.; Saccone, F.; Errandonea, D.; Santamaria-Perez, D.; Segura, A.; Vilaplana, R.; Popescu, C.; Compressibility and structural behavior of pure and Fe-doped SnO_2 nanocrystals. *Sol. State Sci.* **2017**, *64*, 91-98.
28. Ferrari, S.; Bilovol, V.; Pampillo, L.; Grinblat, F.; Saccone, F.; Errandonea, D.; Characterization of V-doped SnO_2 nanoparticles at ambient and high pressures. *Mater. Res. Express* **2018**, *5*, 125005.
29. Ferrari, S.; Pampillo, L.; Saccone, F.; Magnetic properties and environment sites in Fe doped SnO_2 nanoparticles. *Mat. Chem. Phys.* **2016**, *177*, 206-212.

30. Hazen, R.; Finger, L.; Bulk moduli and high-pressure crystal structures of rutile-type compounds. *J. Phys. Chem. Solids* **1981**, *42*, 143-151.
31. Bauer, W.; Rutile type compounds. V. Refinements of MnO_2 and MgF_2. *Acta Crystallogr. B* **1976**, *32*, 2200-2204.
32. Zhang, Z.; Zhou, F.; Lavernia, E.; On the analysis of grain size in bulk nanocrystalline materials via x-ray diffraction. *Metallurgical and Materials Transactions A* **2003**, *34*, 1349-1355.
33. Klotz, S.; Chervin, J.; Munsch, P.; Marchand, G.; Hydrostatic limits of 11 pressure transmitting media. *J. Phys. D: Appl. Phys.* **2009**, *42*, 075413
34. Dewaele, A.; Loubeyre, P.; Mezouar, M.; Equation of state of six metals above 94 GPa. *Phys. Rev. B* **2004**, *70*, 094112.
35. Rodriguez-Carvajal, J.; Recent advances in in magnetic structure determination by neutron powder diffraction. *Physica B* **1993**, *192*, 55-69.
36. Liu, X.F; Gong, W.M.; Iqbal, J.; He, B.; Yu, R.H.; Structural defects-mediated room-temperature ferromagnetism in Co-doped SnO_2 insulating films, *Thin Solid Films* **2009**, *517*, 6091-6095.
37. Gao, Y.; He, J.; Guo, J.; Effect of co-doping and defects on electronic, magnetic, and optical properties in SnO_2: A first-principles study, *Physica B* **2022**, *639*, 413924.
38. Gonzalez-Platas, J.; Alvaro, M.; Nestola, F.; Angel, R.; *EosFit7-GUI*: a new graphical user interface for equation of state calculations, analyses and teaching. *J. Appl. Cryst.* **2016**, *49*, 1377-1382.
39. Haines, J.; Leger, J.; Schulte, O.; The high-pressure phase transition sequence from the rutile-type through to the cotunnite-type structure in PbO_2. *J. Phys. Condens. Matter* **1996**, *8*, 1631.
40. Ross, N.; Shu, J.; Hazen, R.; Gasparik, T.; High-pressure crystal chemistry of stishovite. *Am. Mineral.* **1990**, *75*, 739-747.
41. Errandonea, D.; Muñoz, A.; Gonzalez-Platas, J.; Comment on high pressure x-ray diffraction study of YBO_3/Eu^{3+}, $GdBO_3$, and $EuBO_3$, : Pressure induced amorphization in $GdBO_3$. *J. Applied Physics* **2014**, *115*, 216101.
42. Anzellini, S.; Errandonea, D.; MacLeod, S.; Botella, P.; Daisenberger, D.; De'Ath, M.; Gonzalez-Platas, J.; Ibáñez, J.; McMahon, M.; Munro, K.; Popescu, C.; Ruiz-Fuertes, J.; Wilson, C.; Phase diagram of calcium at high pressure and high temperature. *Phys. Rev. Materials* **2018**, 2, 083608.